Large systems of random linear equations with nonnegative solutions: Characterizing the solvable and the unsolvable phase

Stefan Landmann* and Andreas Engel
Institute of Physics, Carl von Ossietzky University of Oldenburg, D-26111 Oldenburg, Germany

(Received 28 February 2020; accepted 15 May 2020; published 12 June 2020)

Large systems of linear equations are ubiquitous in science. Quite often, e.g., when considering population dynamics or chemical networks, the solutions must be nonnegative. Recently, it has been shown that large systems of random linear equations exhibit a sharp transition from a phase, where a nonnegative solution exists with probability one, to one where typically no such solution may be found. The critical line separating the two phases was determined by combining Farkas' lemma with the replica method. Here we show that the same methods remain viable to characterize the two phases away from criticality. To this end we analytically determine the residual norm of the system in the unsolvable phase and a suitable measure of robustness of solutions in the solvable one. Our results are in very good agreement with numerical simulations.

DOI: 10.1103/PhysRevE.101.062119

I. INTRODUCTION

Systems of linear equations are fundamental objects of study in linear algebra. They play an important role in many fields, ranging from physics to ecology and financial market analysis. In many situations, e.g., when examining the stability of stationary states of systems with a large number of degrees of freedom, one encounters systems with many equations.

In the study of large complex systems it is often not known in detail how the microscopic parts interact with each other. Fortunately, the macroscopic properties frequently do not depend on all of the microscopic details, and it has proven successful to model them by random variables. This is a sensible approach if so-called self-averaging quantities exist that depend only on the parameters of the distributions and not on the individual realizations. A classic example is spin-glass theory [1,2] but also problems from computational complexity [3], information theory [4], and artificial neural networks [5] have been analyzed along these lines.

A natural question occurring when studying large systems of random linear equations concerns their solvability. In some cases this question can be answered easily. Consider a system of linear equations $\hat{a}^T\mathbf{x} = \mathbf{b}$ for the variables $x_\mu \in \mathbb{R}$, $\mu = 1, \ldots, S$ with a real $N \times S$ matrix $\hat{a}^T$ and a real inhomogeneity vector $\mathbf{b} \in \mathbb{R}^N$. In general, this system has a solution if the rank of the matrix, $r(\hat{a}^T)$, is the same as the rank of the augmented matrix, $r(\hat{a}^T|\mathbf{b})$. If the entries of the matrix are drawn independently from a continuous probability distribution, then it has full rank with probability one [6] and the system is almost surely solvable for $S \geqslant N$, i.e., if there are at least as many variables as equations.

In many situations, e.g., when considering models describing population dynamics [7–9], chemical networks [10,11], financial markets [12], or game-theoretic settings [13] the searched-for variables are concentrations or probabilities and must therefore be nonnegative. The question whether a solution $\mathbf{x}$ of the system of linear equations exists with all components x_μ *nonnegative* is nontrivial if $S \geqslant N$.

In Ref. [14] it was shown that this problem may be mapped onto a dual one by using Farkas' lemma [15]. For independent random entries $a_{\mu i}$ and b_i and $S = \mathcal{O}(N)$ the dual problem is amenable to a replica analysis. Remarkably, in the limit $N, S \to \infty$ the system is characterized by a sharp transition from a phase in which a nonnegative solution exists with probability one to one where typically no such solution can be found. The transition line only depends on the statistical properties of the system and is therefore self-averaging.

In Ref. [14] the mapping to the dual problem was used solely to determine the critical line between the two phases. In the present paper we show that it remains valuable also to characterize the system *away* from criticality, i.e., deeply inside the solvable and unsolvable phase, respectively. In this way we get analytic expressions for the remaining variability of the system in the solvable phase as well as for the residual error in the unsolvable one.

The paper is organized as follows. In Sec. II the problem is defined, relevant notation is fixed, and suitable quantities to characterize the two different phases are introduced. Section III contains an intuitive explanation of Farkas' lemma, which is central to this paper. In Sec. IV we sketch the determination of the critical line as performed in Ref. [14]. We then turn to the characterization of the two different phases of the problem and start in Sec. V with the unsolvable phase. Section VI contains the corresponding analysis of the solvable phase. Finally, we summarize our findings in Sec. VII.

II. PROBLEM AND NOTATION

A. Large systems of random linear equations

We study a system of N random linear equations

$$\hat{a}^T\mathbf{x} = \mathbf{b}, \quad \mathbf{x} \geqslant \mathbf{0}, \tag{1}$$

*Corresponding author: stefan.landmann@uni-oldenburg.de

for S unknowns x_μ where the crucial qualification $\mathbf{x} \geqslant \mathbf{0}$ stands for $x_\mu \geqslant 0$ for all $\mu = 1, \ldots, S$. We are hence only looking for solution vectors with *nonnegative* components. The $S \times N$ matrix $\hat{a}$ has independent random entries $a_{\mu i}$ drawn from a Gaussian distribution with average A and variance σ^2,

$$\langle a_{\mu i} \rangle = A, \quad \langle (a_{\mu i} - A)^2 \rangle = \sigma^2, \tag{2}$$

and $\hat{a}^T$ denotes its transpose. The components $b_i, i = 1, \ldots, N$ of the inhomogeneity vector $\mathbf{b}$ are drawn from a Gaussian distribution with average B and variance γ^2/N,

$$\langle b_i \rangle = B, \quad \langle (b_i - B)^2 \rangle = \frac{\gamma^2}{N}. \tag{3}$$

Here and in the following the brackets $\langle \ldots \rangle$ denote the average over the $a_{\mu i}$ and b_i. We are always interested in the large system limit $N \to \infty$ with $S = \alpha N$ and $\alpha = \mathcal{O}(1)$. Note the scaling of the variance $\langle (b_i - B)^2 \rangle \sim 1/N$ with the system size. It is important for a controlled limit $N \to \infty$ in the subsequent calculations.

B. Solvable and unsolvable phase

For $N \to \infty$ the system (1) exhibits a phase transition from a phase where a solution almost always exists to one where typically no such solution can be found. This line depends on the ratio α between the number of variables and the number of equations and on the parameters A, B, σ, and γ of the probability distributions involved. The analytic determination of the transition line was performed in Ref. [14]. To make this paper self-contained and to set the stage for the ensuing calculations the main steps of the corresponding calculations are sketched in Sec. IV. For more details the reader is referred to the original paper.

The central aim of the present work is to characterize the two phases of system (1). To this end we first need to find quantities able to describe relevant properties of the system away from criticality.

In the unsolvable phase no solution $\mathbf{x}$ to (1) exists and it is intuitive to ask "how far" the system is from having a solution. This somewhat vague concept can be quantified by the minimal residual norm:

$$r := \min_{\mathbf{x}, \mathbf{x} \geqslant \mathbf{0}} \left\| \hat{a}^T \mathbf{x} - \mathbf{b} \right\|, \tag{4}$$

where $\| \ldots \|$ denotes the usual quadratic norm of vectors. As long as no solution $\mathbf{x}$ exists r is nonzero. By approaching the solvable phase r should decrease and eventually tend to zero at the transition. We are interested in the detailed behavior of r as a function of α, A, B, σ, and γ.

In the solvable phase the situation is complementary. Now a solution always exists. It is then natural to ask for the robustness or flexibility of the system: How strongly can it be changed or perturbed while still remaining solvable? There are several possibilities to phrase this idea mathematically. One is to determine the *minimal* number of rows $\mathbf{a}_\mu$ and corresponding variables x_μ by which the system (1) has to be reduced such that it is rendered unsolvable. We will discuss related measures in Sec. VI.

III. FARKAS' LEMMA

It is very useful to map the original problem (1) to a dual one with the help of Farkas' lemma [15]. To this end we consider what is called the *nonnegative cone* of row vectors $\mathbf{a}_\mu$ of matrix $\hat{a}$. This cone is spanned by all linear combinations

$$c_1 \mathbf{a}_1 + c_2 \mathbf{a}_2 + \cdots + c_{\alpha N} \mathbf{a}_{\alpha N} \tag{5}$$

of these row vectors with nonnegative coefficients c_μ, cf. Fig. 1. Clearly, if $\mathbf{b}$ falls into this cone, then (1) has a solution whereas no such solution exists when $\mathbf{b}$ lies outside the cone. In the latter case, however, a hyperplane must exist that separates $\mathbf{b}$ from the cone. If we denote the normal of this hyperplane by $\mathbf{y} \in \mathbb{R}^N$, then we may hence state that *either* a solution $\mathbf{x}$ to

$$\hat{a}^T \mathbf{x} = \mathbf{b} \text{ with } \mathbf{x} \geqslant \mathbf{0} \tag{6}$$

exists *or* we may find a vector $\mathbf{y}$ satisfying

$$\hat{a}\mathbf{y} \geqslant \mathbf{0} \text{ and } \mathbf{b} \cdot \mathbf{y} < 0. \tag{7}$$

This duality is the pivotal point of our analysis. As we will show in the next sections (7) may be analyzed using the replica method similar to related problems [16].

IV. DETERMINATION OF THE CRITICAL LINE

Let us first see how we can determine the critical line of the system by studying the inequalities (7). If a vector $\mathbf{y}$ exists which fulfills all inequalities, then the original system (1) does not have solution. If there is no such vector $\mathbf{y}$, then a nonnegative solution $\mathbf{x}$ exists.

To get rid of the trivial degeneracy of solutions $\mathbf{y}$ implied by $\mathbf{y} \to \omega \mathbf{y}$ for any positive ω we first require

$$\|\mathbf{y}\|^2 = \sum_i y_i^2 = N. \tag{8}$$

Next we define the fractional volume $\Omega(\hat{a}, \mathbf{b})$ of all vectors $\mathbf{y}$ which fulfill (7) for given $\hat{a}$ and $\mathbf{b}$:

$$\Omega(\hat{a}, \mathbf{b}) := \frac{\int_{-\infty}^{\infty} \prod_i dy_i \, \delta\left(\sum_i y_i^2 - N\right) \Theta\left(-\frac{1}{\sqrt{N}} \sum_i b_i y_i\right) \prod_\mu \Theta\left(\frac{1}{\sqrt{N}} \sum_i a_{\mu i} y_i\right)}{\int_{-\infty}^{\infty} \prod_i dy_i \, \delta\left(\sum_i y_i^2 - N\right)}. \tag{9}$$

Here Θ denotes Heaviside functions and their arguments have been scaled such that their typical values remain $\mathcal{O}(1)$ for $N \to \infty$.

The geometric interpretation of Ω is depicted in Fig. 2. Due to (8) all vectors $\mathbf{y}$ lie on a sphere with radius $\sqrt{N}$. The inequality $\mathbf{y} \cdot \mathbf{b} < 0$ in (7) constrains them to the lower hemisphere with respect to $\mathbf{b}$. At the same time, all $\mathbf{y}$ need to have a nonnegative scalar product with every row vector of $\hat{a}$. The more variables the system (1) has, the more constraints need to be fulfilled by $\mathbf{y}$. Therefore, the fractional volume

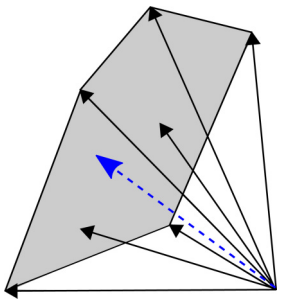

FIG. 1. The geometry of problem (1) in the solvable phase. The inhomogeneity vector **b** (blue dashed) belongs to the cone spanned by nonnegative linear combinations (5) of the row vectors $\mathbf{a}_\mu$ (black solid). Correspondingly, system (1) has a solution **x**. For the situation in the unsolvable phase see Fig. 4.

of solutions (gray shaded area) shrinks, as the number of variables is increased. When the fractional volume becomes zero, there is no **y** satisfying all the inequalities. This implies that a solution to the system (1) exists.

The value of $\Omega(\hat{a}, \mathbf{b})$ depends on the specific choice of the matrix $\hat{a}$ and the vector **b**. Rather than to pinpoint the fractional volume for each individual realization of the randomness we are interested in its *typical* value under the distributions defined in Sec. II. Since Ω is dominated by a *product* of many independent random terms, we cannot expect its average to give a good estimate for its typical value. Instead, this typical value is given by

$$\Omega_{\text{typ}} \simeq \exp\big(\langle \log \Omega \rangle\big). \tag{10}$$

For given statistical parameters A, B, σ, γ the critical line of the transition is determined by finding the value of α for which the *typical value* of the volume Ω becomes zero. Therefore, our quantity of interest is the entropy:

$$S(\alpha, A, B, \sigma, \gamma) := \lim_{N\to\infty} \frac{1}{N} \langle \log \Omega(\hat{a}, \mathbf{b}) \rangle. \tag{11}$$

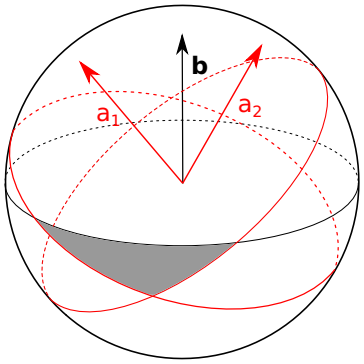

FIG. 2. Volume of allowed solutions **y** of (7) (gray shaded area). All vectors **y** lie on a sphere of radius $\sqrt{N}$. The inequality $\mathbf{y}\cdot\mathbf{b} < 0$ constrains the vectors to lie on the lower hemisphere with respect to **b**. At the same time, they need to have a positive scalar product with all row vectors $\mathbf{a}_\mu$.

For its determination we use the replica trick [17] which is based on the identity:

$$\langle \log \Omega \rangle = \lim_{n\to 0} \frac{\langle \Omega^n \rangle - 1}{n}. \tag{12}$$

The calculation is feasible for $n \in \mathbb{N}$. The result has then to be continued to the real n in order to accomplish the crucial limit $n \to 0$. For $n \in \mathbb{N}$ we have

$$\Omega^n(\hat{a}, \mathbf{b}) = \int_{-\infty}^{\infty} \prod_{i,a} \frac{dy_i^a}{\sqrt{2\pi e}} \prod_a \delta\left[\sum_i (y_i^a)^2 - N\right] \times \prod_{\mu,a} \Theta\left(\frac{1}{\sqrt{N}} \sum_i a_{\mu i} y_i^a\right) \prod_a \Theta\left(-\frac{1}{\sqrt{N}} \sum_i b_i y_i^a\right). \tag{13}$$

Here a is the replica index, which runs from $1 \cdots n$, and the denominators $\sqrt{2\pi e}$ account for the denominator in (9). Replacing the δ and Θ functions by their integral representations the arising integrals can be decoupled by introducing the order parameters:

$$m^a = \frac{1}{\sqrt{N}} \sum_i y_i^a \quad \text{and} \quad q^{ab} = \frac{1}{N} \sum_i y_i^a y_i^b \quad \text{for } a < b. \tag{14}$$

In the limit $N \to \infty$ the integrals may then be calculated by the saddle-point method. Since the solution space of (7) is connected the replica-symmetric ansatz for the saddle point is expected to yield correct results:

$$m^a = m, \quad q^{ab} = q, \quad \text{for } a < b. \tag{15}$$

Some of the resulting saddle-point equations are algebraic and can be used to eliminate the corresponding variables. With the abbreviations

$$Dt := \frac{dt}{\sqrt{2\pi}} e^{-t^2/2}, \quad H(x) := \int_x^\infty Dt, \tag{16}$$

as well as

$$\kappa := \frac{mA}{\sigma}, \quad \lambda := \frac{\sigma B}{\gamma A}, \tag{17}$$

we finally arrive at [14]

$$S(\alpha, \lambda) = \text{extr}_{q,\kappa}\left[\frac{1}{2}\log(1-q) + \frac{q}{2(1-q)} - \frac{\lambda^2}{2}\frac{\kappa^2}{1-q} + \alpha \int Dt \, \log H\left(\frac{\sqrt{q}\,t - \kappa}{\sqrt{1-q}}\right)\right]. \tag{18}$$

The order parameter q characterizes the typical overlap between two different solutions **y** from the solution space. It varies from $q = 0$ for $\alpha = 0$ to $q \to 1$ close to the phase transition. To determine the transition line we may hence reduce Eq. (18) to its most divergent terms for $q \to 1$. In this limit we have

$$\int Dt \, \log H\left(\frac{\sqrt{q}\,t - \kappa}{\sqrt{1-q}}\right) \sim -\frac{1}{2(1-q)} \int_\kappa^\infty Dt \, (t-\kappa)^2 =: -\frac{1}{2(1-q)} I(\kappa) \tag{19}$$

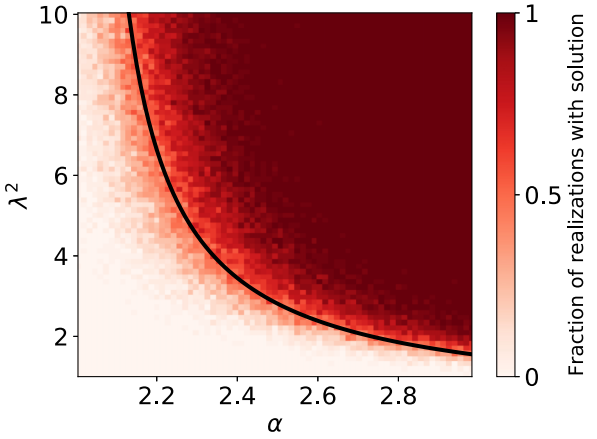

FIG. 3. The transition from the unsolvable to the solvable phase in dependence of the statistical properties of the random variables described by λ and the ratio α between the number of variables and the number of equations. The color indicates the fraction of randomly drawn systems (1) for which a nonnegative solution could be found numerically. The black line shows the analytical prediction of the critical line given by Eqs. (21) and (22). Parameters: $N = 300$, every data point shows the average over 50 realizations.

and correspondingly get

$$S(\alpha_c, \lambda) \sim \mathrm{extr}_{q,\kappa} \left[\frac{1}{2(1-q)} - \frac{\lambda^2}{2} \frac{\kappa^2}{(1-q)} - \frac{\alpha_c}{2(1-q)} I(\kappa) \right]. \quad (20)$$

The critical value α_c of α is determined by the remaining saddle-point equations for q and κ:

$$1 - \lambda^2 \kappa^2 = \alpha_c I(\kappa), \quad (21)$$

$$\alpha_c H(\kappa) = 1. \quad (22)$$

Note that in this result the statistical properties of $a_{\mu i}$ and b_i as specified by the parameters A, B, σ, and γ only arise in form of λ defined in (17) which gives the scaled ratio of the relative variances of $a_{\mu i}$ and b_i.

Figure 3 shows the critical line (black) given by (21) and (22) in comparison with simulation results. The color indicates the fraction of randomly drawn systems for which a nonnegative solution could be found using a nonnegative least-squares solver [18]. There is good agreement between the analytical prediction and the numerics.

V. THE UNSOLVABLE PHASE

In the unsolvable phase of problem (1) no solution vector $\mathbf{x}$ may be found. In Sec. II we proposed the residual norm r defined in (4) as a measure of how far the system is from having a solution. We will show now how to determine the typical value of r from the dual problem (7). To this end it is useful to first give r a geometrical interpretation, see Fig. 4. In the unsolvable phase the inhomogeneity vector $\mathbf{b}$ lies outside the cone of possible nonnegative linear combinations $\hat{a}^T\mathbf{x}$.

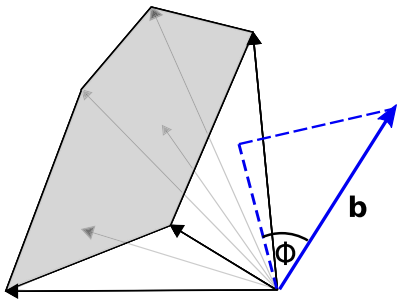

FIG. 4. In the unsolvable phase the inhomogeneity vector $\mathbf{b}$ lies outside the cone of possible nonnegative linear combinations $\hat{a}^T\mathbf{x} = \sum_\mu^S x_\mu \mathbf{a}_\mu$. The minimal residual norm $r = \min_{\mathbf{x},\mathbf{x}\geqslant\mathbf{0}} \|\hat{a}^T\mathbf{x} - \mathbf{b}\|$, is realized by a linear combination which lies on the face of the cone closest to $\mathbf{b}$. Therefore, it is completely determined by the smallest angle $\phi_{\min}$ between the cone and $\mathbf{b}$.

The best approximation to $\mathbf{b}$ by a vector $\hat{a}^T\mathbf{x}$ of the cone lies on a face of this cone and realizes the smallest possible angle $\phi_{\min}$ between $\mathbf{b}$ and the surface of the cone. We hence get $r = b\sin(\phi_{\min})$ with $b = \|\mathbf{b}\|$.

It remains to find a way to determine $\phi_{\min}$ from the dual problem involving the vectors $\mathbf{y}$. Since there is no solution to equation (1) there is at least one and in fact several hyperplanes separating the cone from $\mathbf{b}$. The angle between these hyperplanes and $\mathbf{b}$ ranges from 0 (when the hyperplane contains $\mathbf{b}$) to $\phi_{\min}$ (when the hyperplane contains the face of the cone closest to $\mathbf{b}$). Any hyperplane having an angle with $\mathbf{b}$ larger than $\phi_{\min}$ violates at least one of the constraints in $\hat{a}\mathbf{y} \geqslant \mathbf{0}$. Thus, we can determine $\phi_{\min}$ by finding the hyperplane fulfilling the constraints given by Farkas' lemma and making the *largest possible* angle with $\mathbf{b}$. In terms of normal vectors $\mathbf{y}$ this is equivalent to

$$r = \max_{\mathbf{y}} \left(-\frac{1}{\sqrt{N}} \mathbf{y} \cdot \mathbf{b} \right), \quad (23)$$

where the maximum is over all vectors $\mathbf{y}$ fulfilling

$$\hat{a}\mathbf{y} \geqslant \mathbf{0} \ , \quad \mathbf{b}\cdot\mathbf{y} < 0, \quad \|\mathbf{y}\|^2 = N. \quad (24)$$

This formulation allows to determine the typical value of r by a slight extension of the methods described in Sec. IV, see also Ref. [19] for a related situation. The procedure is best explained by comparing Figs. 2 and 5. In order to determine r we have to find the maximal value $\eta_{\max}$ of

$$\eta := -\frac{1}{\sqrt{N}} \mathbf{y} \cdot \mathbf{b}, \quad (25)$$

in the shaded solution space Ω. We proceed as follows: We first fix a value of η thereby constraining the vectors $\mathbf{y}$ to lie on a given latitude shown by the dotted blue line in Fig. 5. The part of this line inside Ω (full blue line) represents those vectors $\mathbf{y}$ that belong to Ω and make the required angle with $\mathbf{b}$. As η increases the full blue line gets shorter and shorter. It shrinks to a point at the "most southern tip" of the solution space when the maximal possible value $\eta_{\max}$ of η has been

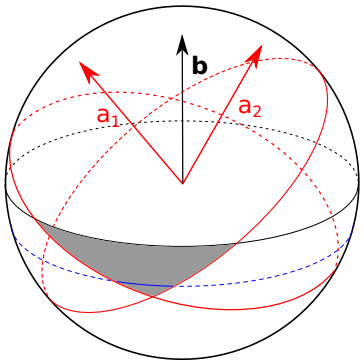

FIG. 5. Solution volume Ω (gray shaded) as in Fig. 2 together with the locus of vectors **y** making a definite angle with **b** (horizontal blue line, solid and dashed), cf. Eq. (25). At the maximum value of this angle the line hits the "southern tip" of the gray area.

reached. We may therefore determine $\eta_{\max}$ by calculating the modified fractional volume $\tilde{\Omega}(\hat{a}, \mathbf{b}, \eta)$ including the constraint (25) and looking for the value of η for which it goes to zero.

The modified fractional volume $\tilde{\Omega}(\hat{a}, \mathbf{b}, \eta)$ is obtained from $\Omega(\hat{a}, \mathbf{b})$ as defined in (9) by the mere replacement

$$\Theta\left(-\frac{1}{\sqrt{N}}\sum_i b_i y_i\right) \longrightarrow \delta\left(-\frac{1}{\sqrt{N}}\sum_i b_i y_i - \eta\right). \tag{26}$$

The explicit calculations are hence rather similar to Sec. IV. They yield the following expression for the corresponding entropy

$$\begin{aligned}\tilde{S}(\alpha, \lambda, \eta/\gamma) &= \lim_{N\to\infty}\frac{1}{N}\langle \log \tilde{\Omega}(\hat{a}, \mathbf{b}, \eta)\rangle \\ &= \mathrm{extr}_{q,\kappa}\left[\frac{1}{2}\log(1-q) + \frac{q}{2(1-q)} - \frac{(\eta/\gamma + \kappa\lambda)^2}{2(1-q)} + \alpha\int Dt\ \log H\left(\frac{\sqrt{q}\,t-\kappa}{\sqrt{1-q}}\right) + C\right],\end{aligned} \tag{27}$$

where C is an irrelevant constant arising from the different normalizations of $\Omega(\hat{a}, \mathbf{b})$ and $\tilde{\Omega}(\hat{a}, \mathbf{b}, \eta)$.

The limit $\tilde{\Omega} \to 0$ is again accompanied by $q \to 1$. Keeping only the most divergent terms we find

$$\tilde{S}(\alpha, \lambda, \eta_{\max}/\gamma) = \mathrm{extr}_{q,\kappa}\left[\frac{1}{2(1-q)} - \frac{(\eta_{\max}/\gamma + \kappa\lambda)^2}{2(1-q)} - \frac{\alpha}{2(1-q)} I(\kappa)\right], \tag{28}$$

with the corresponding saddle-point equations

$$\begin{aligned} 1 - (\eta_{\max}/\gamma + \kappa\lambda)^2 &= \alpha\, I(\kappa), \\ \kappa\lambda(\eta_{\max}/\gamma + \kappa\lambda) &= \alpha[H(\kappa) - I(\kappa)]. \end{aligned} \tag{29}$$

Here H and I denote the functions defined in (16) and (19), respectively. From the numerical solutions to (29) we get our final result $r = \eta_{\max}$.

Figure 6 compares results for r obtained in this way with numerical simulations for systems of size $N = 1000$. The data points were generated by averaging over 10 realizations of the randomness. For each realization the minimal residual norm r of the random system Eq. (1) was determined using a least-squares solver [18]. There is very good agreement between numerics and analytical results. The qualitative behavior is as expected: In the unsolvable phase, $\alpha < \alpha_c$, the minimal residual norm is nonzero. It monotonically decreases as the system approaches α_c to eventually reach zero at $\alpha = \alpha_c$.

VI. THE SOLVABLE PHASE

Similar to the previous section we now try to characterize the solvable phase of (1) by using the dual picture (7). In the solvable phase, it is not possible to find a vector **y** which fulfills all inequalities in (7) simultaneously. We may then ask for the best **y** that violates the inequalities $\hat{a}\mathbf{y} \geqslant \mathbf{0}$ the least. To formalize the idea let us define a cost function

$$v(\mathbf{y}) = \sum_\mu E(\Delta_\mu), \quad \Delta_\mu := \frac{1}{\sqrt{N}}\sum_i a_{\mu i} y_i, \tag{30}$$

which assigns an "energy" E to each violated constraint.

The choice of the cost function depends on the problem under consideration. For concreteness, we consider two typical examples which are compared in Fig. 7. The first one derives from the step function

$$E(\Delta_\mu) = \Theta(-\Delta_\mu), \tag{31}$$

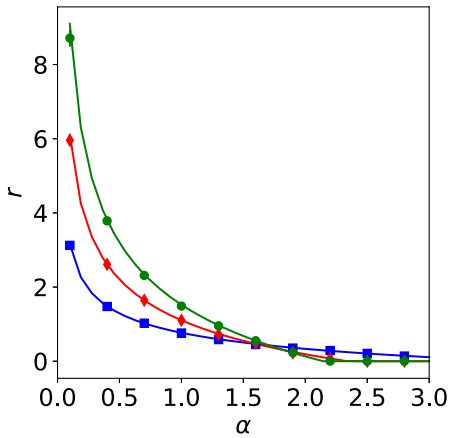

FIG. 6. Comparison of analytical results and numerical simulations for the residual error r in the unsolvable phase. The standard deviations of the numerical results are smaller than the symbol size. Parameters: $A = B = \gamma = 1$, $\sigma = 1, 2, 3$ (blue squares, red diamonds, green circles), $N = 1000$, averaged over 10 realizations for each data point.

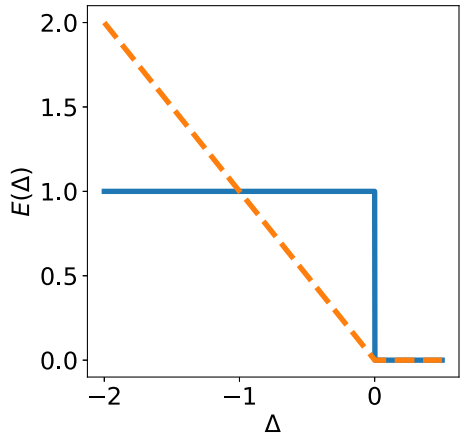

FIG. 7. The two cost functions studied in this section: The step function defined in (31) (blue solid) and the ramp function (32) (orange dashed).

and simply counts the number of violated constraints. Its minimum over all choices of $\mathbf{y}$ hence corresponds to the minimal number of row vectors $\mathbf{a}_\mu$ that have to be eliminated from $\hat{a}$ such that a solution $\mathbf{y}$ exists. Going back to the original problem it therefore gives the minimal number of row vectors $\mathbf{a}_\mu$ and corresponding variables x_μ by which the system (1) has to be reduced such that it does not possess a nonnegative solution anymore. In view of Fig. 1 this number gives an estimate for the number of "crucial" row vectors $\mathbf{a}_\mu$ that are indispensable for the cone to contain $\mathbf{b}$.

The second cost function builds on the ramp function

$$E(\Delta_\mu) = -\Theta(-\Delta_\mu)\,\Delta_\mu \tag{32}$$

and is sensitive not only to the violation of a constraint per se but also to the value of Δ_μ, i.e., to the strength of such a violation [20]. Referring again to Fig. 1 its minimal value characterizes the sensitivity of the system (1) to small variations in $\hat{a}$ and $\mathbf{b}$ because it indicates whether $\mathbf{b}$ lies "well in the middle" of the nonnegative cone of the $\mathbf{a}_\mu$ or rather near to its boundary.

It is again possible to calculate the typical minimal values of both cost functions within the replica approach outlined above. To this end we introduce an auxiliary inverse temperature β and define the partition function

$$Z(\hat{a}, \mathbf{b}, \beta) = \frac{\int \prod_i dy_i \delta\left(\sum_i y_i^2 - N\right) \Theta\left(-\frac{1}{\sqrt{N}} \sum_i b_i y_i\right) \exp\left[-\beta v(\mathbf{y})\right]}{\int \prod_i dy_i \delta\left(\sum_i y_i^2 - N\right)}. \tag{33}$$

It is instructive to compare this expression with the fractional volume, Eq. (9), which was used to examine the phase transition and the minimal residual norm in the unsolvable phase. There, only those $\mathbf{y}$ contributed to the integral which do not violate any constraint at all in $\hat{a}\mathbf{y} \geqslant \mathbf{0}$, i.e., only those with $v(\mathbf{y}) = 0$. The entropy (11) was hence similar to a microcanonical ground-state entropy. Complementary, Eq. (33) is like a canonical partition function to which all $\mathbf{y}$ contribute, also those violating the constraints, albeit suppressed by the Boltzmann factor $\exp[-\beta v(\mathbf{y})]$. The role of the entropy in the microcanonical approach is now taken by the free energy

$$F(\alpha, \lambda, \beta) := -\lim_{N\to\infty} \frac{1}{\alpha N \beta} \langle \log Z(\hat{a}, \mathbf{b}, \beta) \rangle. \tag{34}$$

The minimal possible average cost per equation $\langle E_{\min} \rangle$ corresponds to the ground-state energy and is given as the low temperature limit of the free energy:

$$\langle E_{\min} \rangle = \frac{\langle v_{\min} \rangle}{\alpha N} = \lim_{\beta\to\infty} F(\alpha, \lambda, \beta). \tag{35}$$

Its calculation is yet another variation of the one sketched in Sec. IV and proceeds along the lines of Refs. [16,21,22]. The same order parameters are defined as in (14) and under the assumption of replica symmetry, we find

$$F(\alpha, \lambda, \beta) = \mathrm{extr}_{q,\kappa} \left[-\frac{\log(1-q)}{2\alpha\beta} - \frac{q}{2\alpha\beta(1-q)} + \frac{\lambda^2\kappa^2}{2\alpha\beta(1-q)} - \frac{1}{\beta} G_E \right], \tag{36}$$

where

$$G_E = \int Dt \log \int d\Delta \times \exp\left[-\beta E(\Delta) - \frac{(\Delta/\sigma - \kappa + t\sqrt{q})^2}{2(1-q)} \right]. \tag{37}$$

The limit $\beta \to \infty$ to project out the ground state is accompanied by $q \to 1$ such that $x := \beta(1-q)$ remains of $\mathcal{O}(1)$. In this limit, therefore, the role of the saddle-point variable q is taken over by x. In this way G_E becomes

$$G_E = \beta \int Dt \left[-E(\Delta_0) - \frac{(\Delta_0/\sigma - \kappa + t)^2}{2x} \right], \tag{38}$$

where

$$\Delta_0(t) = \arg\min_\Delta \left[E(\Delta) + \frac{(\Delta/\sigma - \kappa + t)^2}{2x} \right]. \tag{39}$$

For the step cost function (31) the minimum is realized by

$$\Delta_0(t) = \begin{cases} \sigma(\kappa - t) & \text{if } t < \kappa \\ 0 & \text{if } \kappa \leqslant t \leqslant \kappa + \sqrt{2x}. \\ \sigma(\kappa - t) & \text{if } t > \kappa + \sqrt{2x} \end{cases} \tag{40}$$

The typical minimal cost per equation is then given by

$$\langle E_{\min} \rangle = \mathrm{extr}_{x,\kappa} \left[-\frac{1}{2\alpha x} + \frac{\lambda^2\kappa^2}{2\alpha x} + H\left(\kappa + \sqrt{2x}\right) + \frac{1}{2x} \int_\kappa^{\kappa+\sqrt{2x}} Dt\, (t-\kappa)^2 \right]. \tag{41}$$

This expression is similar to the one for the minimal fraction of misclassified patterns of a perceptron [21,22]. Here, however, we have the additional term $\frac{\lambda^2\kappa^2}{2x}$ and the additional extremization in κ.

The saddle-point equations corresponding to (41) read

$$\alpha \int_\kappa^{\kappa+\sqrt{2x}} Dt\, (t-\kappa)^2 = 1 - \lambda^2\kappa^2, \tag{42}$$

$$\alpha \int_\kappa^{\kappa+\sqrt{2x}} Dt\, (t-\kappa) = \lambda^2\kappa, \tag{43}$$

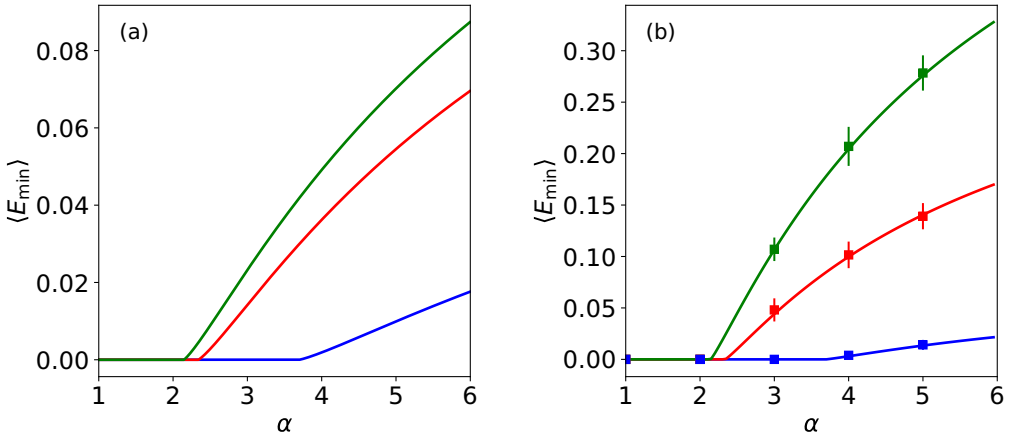

FIG. 8. The lines show the typical minimal energy $\langle E_{\min}\rangle$ for the step cost function (a) and for the ramp cost function (b) as given by Eq. (44) and (50), respectively. Parameters: $A = B = \gamma = 1$, and $\sigma = 1, 2, 3$ (blue bottom, red middle, green top). Each symbol of the numerical results for the ramp function was generated from systems with $N = 300$ and averaged over 25 realizations. The error bars show the standard deviation.

and (41) simplifies to

$$\langle E_{\min}\rangle = H(\kappa + \sqrt{2x}). \tag{44}$$

Note that κ and x in this expression have to be determined from the numerical solution of the saddle-point equations (42) and (43).

Analytical results for $\langle E_{\min}\rangle$ in case of the step cost function as function of α are shown in Fig. 8(a). The overall behavior is as expected: For α below the critical value α_c, the system is in the unsolvable phase, all constraints in (7) can be fulfilled and $\langle E_{\min}\rangle$ is zero. For $\alpha > \alpha_c$ some of the constraints can no longer be fulfilled and $\langle E_{\min}\rangle$ starts to monotonically grow. Since the determination of $\langle E_{\min}\rangle$ by simulations is computationally very demanding and not indispensable for this work we have refrained from doing so.

For the ramp cost function (32) the calculation is similar. Equation (40) is modified to

$$\Delta_0(t) = \begin{cases} \sigma(\kappa - t) & \text{if } t < \kappa \\ 0 & \text{if } \kappa \leqslant t \leqslant \kappa + \sigma x \\ \sigma(x\sigma + \kappa - t) & \text{if } t > \kappa + \sigma x \end{cases} \tag{45}$$

and G_E acquires the form

$$\frac{G_E}{\beta} = -\frac{1}{2x}\int_{\kappa}^{\kappa+x\sigma} Dt\,(\kappa - t)^2 + \sigma\Big(\kappa + \frac{x\sigma}{2}\Big)H(\kappa + x\sigma) - \frac{\sigma}{\sqrt{2\pi}}\exp\left[-\frac{(\kappa + x\sigma)^2}{2}\right]. \tag{46}$$

The typical minimal cost per equation becomes

$$\langle E_{\min}\rangle = \mathrm{extr}_{x,\kappa}\left\{-\frac{1}{2\alpha x} + \frac{\lambda^2\kappa^2}{2\alpha x} - \sigma\Big(\kappa + \frac{x\sigma}{2}\Big)H(\kappa + x\sigma) + \frac{1}{2x}\int_{\kappa}^{\kappa+x\sigma} Dt(\kappa - t)^2 + \frac{\sigma}{\sqrt{2\pi}}\exp\left[-\frac{(\kappa + x\sigma)^2}{2}\right]\right\}, \tag{47}$$

complemented by the saddle-point equations

$$1 - \lambda^2\kappa^2 = \alpha\sigma^2x^2H(\kappa + \sigma x) + \alpha\int_{\kappa}^{\kappa+x\sigma} Dt(\kappa - t)^2, \tag{48}$$

$$\lambda^2\kappa = \alpha x\sigma H(k + \sigma x) - \alpha\int_{\kappa}^{\kappa+x\sigma} Dt(\kappa - t). \tag{49}$$

The final result for the typical minimal cost per equation assumes the form

$$\langle E_{\min}\rangle = -\sigma(\kappa + x\sigma)H(\kappa + x\sigma) + \frac{\sigma}{\sqrt{2\pi}}e^{-(\kappa+x\sigma)^2/2}, \tag{50}$$

where again the values of the saddle-point variables κ and x as determined from the numerical solution of (48) and (49) have to be plugged into this expression.

In Fig. 8(b) analytical and numerical results for $\langle E_{\min}\rangle$ for the ramp cost function are compared. In this case, it is straightforward to get numerical results since the minimal value of $v(\mathbf{y})$ can be determined using standard tools as the scipy.optimize.minimize function in Python. Very good agreement between analytical and numerical results is found.

The results on the minimal cost per equation shown in Fig. 8 can be specified in more detail by determining the distribution $p_{\min}(\Delta)$ of the "violation strengths" Δ_μ defined in (30) in the limit $\beta \to \infty$. In Ref. [22] it is shown that this distribution is given by

$$p_{\min}(\Delta) = \int Dt\,\delta[\Delta - \Delta_0(t)]. \tag{51}$$

In this way we find for the step cost function

$$p_{\min}(\Delta) = \delta(\Delta)\int_{\kappa}^{\kappa+\sqrt{2x}} Dt + \Big[\Theta(\Delta) + \Theta(-\Delta - \sigma\sqrt{2x})\Big]\frac{1}{\sqrt{2\pi}\sigma}e^{-(\kappa - \frac{\Delta}{\sigma})^2/2} \tag{52}$$

and for the ramp function

$$p_{\min}(\Delta) = \delta(\Delta)\int_{\kappa}^{\kappa+\sigma x} Dt + \Theta(\Delta)\frac{1}{\sqrt{2\pi}\sigma}e^{-(\kappa - \frac{\Delta}{\sigma})^2/2} + \Theta(-\Delta)\frac{1}{\sqrt{2\pi}\sigma}e^{-(-\frac{\Delta}{\sigma} + \sigma x + \kappa)^2/2}. \tag{53}$$

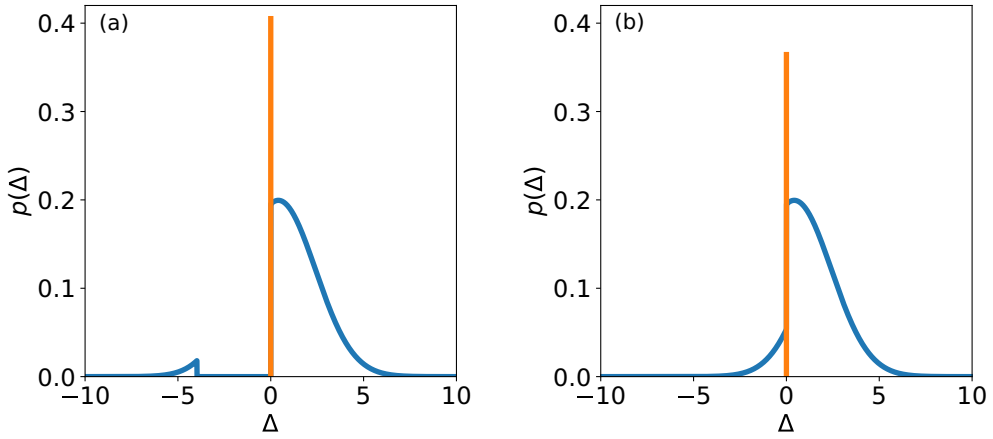

FIG. 9. Left: Distribution of violation strengths Δ for the step function (a) and the ramp function (b). The height of the line at $\Delta = 0$ gives the prefactor of the respective δ function. Parameters: $A = B = \gamma = 1, \sigma = 2, \alpha = 3$.

Figure 9 compares these two distributions in the interesting regime $\alpha > \alpha_c$. Figure 9(a) shows $p_{\min}$ for the step function. The δ peak at $\Delta = 0$ is caused by constraints that are fulfilled as equalities, whereas the part of the Gaussian for $\Delta > 0$ represents constraints which are more than just barely fulfilled. Note the gap of width $\sigma\sqrt{2x}$ in the negative part of the distribution. This gap is due to the fact that the step cost function does not differentiate between heavily violated constraints and those only slightly violated. It therefore prefers few "gross mistakes" to many tiny ones. In this way it selects the row vectors $\mathbf{a}_\mu$ that are "most crucial" for the cone to contain the vector $\mathbf{b}$ as discussed at the beginning of this section. In contrast, the distribution $p_{\min}(\Delta)$ for the ramp cost function is gapless, see Fig. 9(b). Since the ramp function punishes strong violations of constraints more severely than slight violations its optimal value is realized with many but small violations. It therefore characterizes some average distance of $\mathbf{b}$ from the boundary of the cone. No gap in the distribution is therefore to be expected. Note that the typical minimal cost per equation is recovered from the distributions $p_{\min}(\Delta)$ by:

$$\langle E_{\min}\rangle = \int d\Delta\, E(\Delta)\, p_{\min}(\Delta). \tag{54}$$

VII. CONCLUSION

Large systems of random linear equations exhibit intriguing properties if their variables are constrained to be nonnegative. These systems show a sharp transition from a phase where a solution can be found with probability one to a phase where typically no such solution exists. The transition line depends only on the statistical properties of the systems and is hence self-averaging.

In the present paper we showed that the mapping used in Ref. [14] to determine the critical line is also the clue to characterize the two phases away from criticality. To this end we introduced suitable quantities describing the phases and determined their typical values as function of the statistical parameters of the random ensembles and the ratio between the number of variables and the number of equations. The unsolvable phase can be characterized by the typical residual norm of the system of equations. It measures how 'far away' the system is from being solvable. In the solvable phase two measures for the robustness of solutions were introduced and analyzed.

Our analytical investigations became possible by first mapping the problem onto a dual one using Farkas' lemma and then analyzing this dual problem with the help of the replica method. Technically, our results depend on the correctness of the assumption of replica symmetry. In the unsolvable phase, $\alpha \leqslant \alpha_c$, the solution space of the dual problem is connected and it is reasonable to expect replica symmetry to hold. On the other hand, the solvable phase is characterized by a disconnected solution space of the dual problem and replica symmetry breaking may come into play [21–23].

ACKNOWLEDGMENTS

We thank Mattes Heerwagen and Sebastian Rosmej for fruitful discussions and Imre Kondor for interesting correspondence. Financial support from the German Science Foundation under Project No. 317605153 is gratefully acknowledged.

[1] S. F. Edwards and P. W. Anderson, J. Phys. F: Met. Phys. **5**, 965 (1975).
[2] D. Sherrington and S. Kirkpatrick, Phys. Rev. Lett. **35**, 1792 (1975).
[3] R. Monasson, R. Zecchina, S. Kirkpatrick, B. Selman, and L. Troyansky, Nature **400**, 133 (1999).
[4] M. Mezard and A. Montanari, *Information, Physics, and Computation* (Oxford University Press, Oxford, 2009).
[5] A. Engel and C. Van den Broeck, *Statistical Mechanics of Learning* (Cambridge University Press, Cambridge, UK, 2001).
[6] X. Feng and Z. Zhang, Appl. Math. Comput. **185**, 689 (2007).

[7] R. M. May, Nature **238**, 413 (1972).
[8] M. Eigen and P. Schuster, Naturwissenschaften **65**, 7 (1978).
[9] M. Tikhonov and R. Monasson, Phys. Rev. Lett. **118**, 048103 (2017).
[10] M. Polettini and M. Esposito, J. Chem. Phys. **141**, 024117 (2014).
[11] J. Schnakenberg, J. Theor. Biol. **81**, 389 (1979).
[12] I. Kondor, G. Papp, and F. Caccioli, J. Stat. Mech.: Theory Exp. (2017) 123402.
[13] J. Berg and A. Engel, Phys. Rev. Lett. **81**, 4999 (1998).
[14] S. Landmann and A. Engel, Physica A: Stat. Mech. Appl. **552**, 122544 (2020).
[15] J. Farkas, J. reine angew. Math. **124**, 1 (1902).
[16] E. Gardner, J. Phys. A: Math. Gen. **21**, 257 (1988).
[17] M. Mézard, G. Parisi, and M. Virasoro, *Spin Glass Theory and Beyond* (World Scientific, Singapore, 1987).
[18] We used the nonnegative least-squares solver nnls from the scipy.optimize package in Python.
[19] A. Engel and C. Van den Broeck, Phys. Rev. Lett. **71**, 1772 (1993).
[20] Both functions have an equivalent in the theory of neural networks: The step function corresponds to the Gardner-Derrida cost function [21], the ramp function to the perceptron cost function [22].
[21] E. Gardner and B. Derrida, J. Phys. A: Math. Gen. **21**, 271 (1988).
[22] M. Griniasty and H. Gutfreund, J. Phys. A: Math. Gen. **24**, 715 (1991).
[23] M. Bouten and B. Derrida, J. Phys. A: Math., Nucl. Gen. **27**, 6021 (1994).